Materials Letters 345 (2023) 134485

Contents lists available at ScienceDirect

Materials Letters

journal homepage: www.elsevier.com/locate/matlet

Complex dielectric function of H-free *a*-Si films: Photovoltaic light absorber

E. Marquez [a,*], M. Ballester [b], M. Garcia [a], M. Cintado [a], A.P. Marquez [a], J.J. Ruiz [a], S.M. Fernández [c], E. Blanco [a], F. Willomitzer [d], A.K. Katsaggelos [b]

[a] University of Cadiz, 11510 Puerto Real, Spain
[b] Northwestern University, 633 Clark St, Evanston, IL 60208, USA
[c] CIEMAT, Avenida Complutense 40, 28040 Madrid, Spain
[d] Wyant College of Optical Sciences, University of Arizona, Tucson, AZ 85721 USA

ARTICLE INFO

Keywords:
Amorphous materials
Optical materials and properties

ABSTRACT

a-Si layers could serve as a low-cost precursor for fabricating a poly-Si absorber for photovoltaic cells. We prepared *a*-Si films onto glass substrates by RF-magnetron sputtering. The Ar-gas pressure was adjusted from 0.7 to 4.5 Pa to reach average rates ($\gtrsim$1.0 nm/s), and increase manufacturing efficiency. We analyzed the structural and optical properties of the *a*-Si films using Raman and optical transmission spectroscopies. The Cody-Lorentz model was adopted to calculate their complex refractive index.

1. Introduction

Silicon is the most-frequently-used material in the fabrication of photovoltaic cells and an essential element for the solar-cell industry. It is also one of the most-abundant materials on Earth, not toxic, and shows excellent stability. Around 90 % of the manufactured photovoltaic cells employ *a*-Si. Nowadays, efforts are focused on searching for *inexpensive* alternatives to replace previous technologies. Among them, poly-Si is a promising material that can be fabricated in thin films using *unhydrogenated* *a*-Si as a precursor in CW-diode-laser treatment [1]. Prior knowledge on the dielectric properties of the precursor becomes relevant for its effect on the subsequent properties of poly-Si.

The optical functions of RF-magnetron-sputtering *a*-Si films strongly depend on the deposition conditions used in their preparation. This relation is well-documented in the literature, which shows a correlation between the *void* volume fraction and RF power. Given these complexities and the relative lack of research on unhydrogenated *a*-Si, we considered it inappropriate to solely use the widespread literature data.

This research reports the structural and optical characterizations of *a*-Si films prepared by RFMS. The Kramers–Kronig (KK)-consistent Cody-Lorentz (CL)-oscillator model has been selected to calculate the average thickness, $\overline{d}$, thickness variation, Δd, refractive index, n, extinction coefficient, k, and the real and imaginary parts of the dielectric function, ϵ_1 and ϵ_2, respectively. Spectroscopic ellipsometry is commonly used to determine optical properties in the spectral regions of higher absorption. For our near-gap-region of interest [2], the transmission provides more accurate and precise results.

2. Experiments

a-Si layers were grown onto room-temperature glass substrates using an RFMS MVSystem. The *a*-Si films were deposited with a power of 525 W and an Ar-gas pressure ranging from 0.7 to 4.5 Pa. These selected conditions obtain the highest average rate $\gtrsim$1.0 nm/s.

We studied the structural properties of the *a*-Si using AFM, SEM, and Raman spectroscopy. Fig. 1*a* shows the surface roughness measured with AFM. The representative specimen #1 displayed exhibits an RMSE surface roughness of 1.55 nm. The normal-incidence transmittance spectra were acquired with a Perkin-Elmer Lambda-1050 UV/visible/NIR spectrophotometer. We have chosen the spectral region where the dispersive glass substrate is *nonabsorbing*.

3. Cody-Lorentz function

The CL model defines the imaginary part of the dielectric function as [3]:

$$\epsilon_2(E) = \begin{cases} \dfrac{E_t}{E} G(E_t) L(E_t) \exp\left(\dfrac{E - E_t}{E_u}\right), & 0 < E \leqslant E_t, \\ G(E) L(E) = G(E) \dfrac{A E_0 \Gamma E}{\left(E^2 - E_0^2\right)^2 + \Gamma^2 E^2}, & E > E_t, \end{cases} \quad (1)$$

* Corresponding author.
E-mail address: emilio.marquez@uca.es (E. Marquez).

https://doi.org/10.1016/j.matlet.2023.134485
Received 14 February 2023; Received in revised form 7 April 2023; Accepted 30 April 2023
Available online 6 May 2023

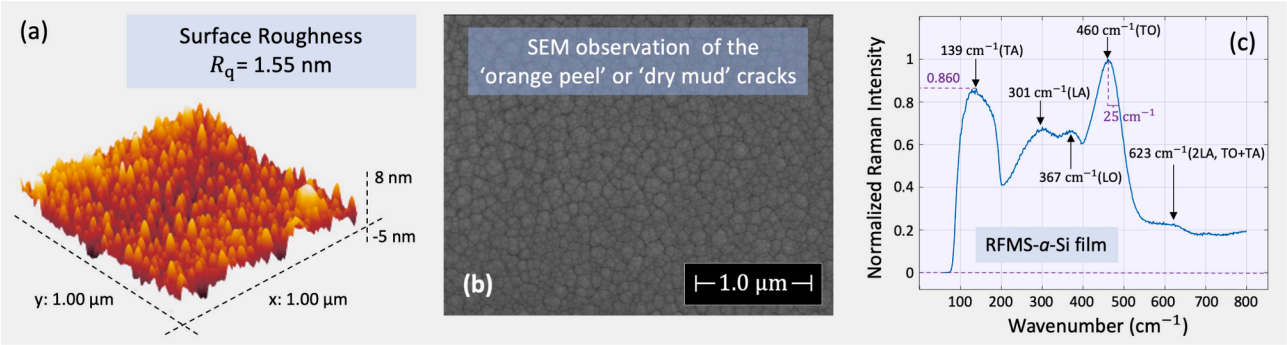

Fig. 1. (a) AFM and (*b*) top-view-SEM-image of *a*-Si. (*c*) Raman spectrum.

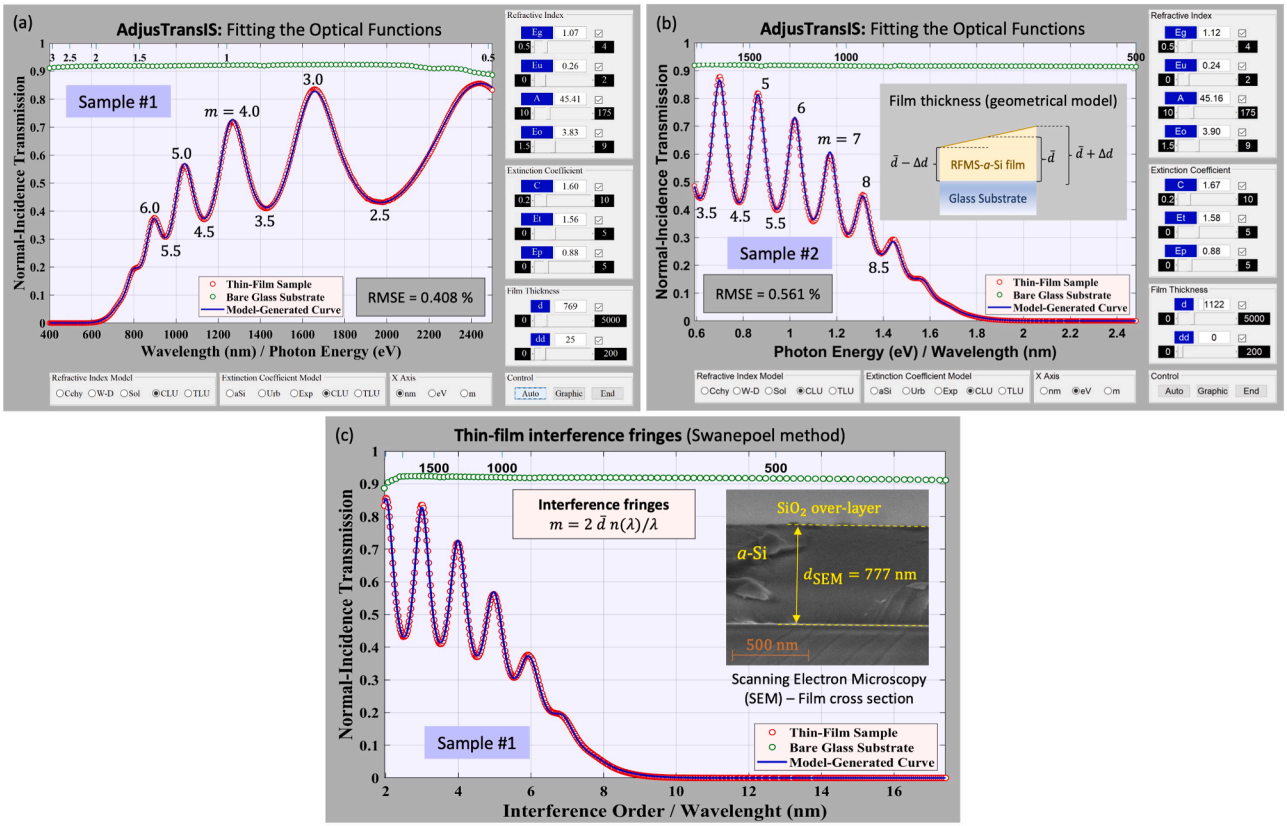

Fig. 2. 'AdjusTransIS' GUI comparing simulated and experimental spectra for (*a*) sample #1, (*b*) sample #2. (*c*) Transmittance *versus m*, showing the envelope-method tangential points. Insets show the cross-sectional-SEM-image and sample geometry. The fitted parameters are indicated in their respective GUIs.

where E_t is the transition energy between the Urbach tail, and the band-to-band transitions, and ϵ_2 includes the product of the Lorentz-oscillator function, $L(E)$, with a band-edge function, $G(E)$. A represents the amplitude, E_0 the resonance energy, and Γ the width. The real part of the dielectric function, $\epsilon_1(E)$, is found from the KK-transformation of $\epsilon_2(E)$.

Eq. 1 generalizes the Tauc-Lorentz [4] model, adding the Urbach tail and a new function $G(E)$, chosen for consistency with the absorption onset. The Tauc expression defines $G_T(E) = [(E-E_g)/E]^2$, and it was derived upon the assumptions of parabolic bands and constant-*momentum*-matrix element. The Cody-Lorentz empirical expression is given by: $G_c(E) = (E-E_g)^2/[(E-E_g)^2 + E_p^2]$. E_p defines a second transition energy at $E_g + E_p$ that separates the absorption onset from the Lorentz-oscillator behavior, providing a flexibility lacking in the Tauc-Lorentz approach [4]. If $E \approx E_g$, then $G_0 \rightarrow [(E-E_g)/E_p]^2$, a formula consistent with the assumptions of parabolic bands and a constant-*dipole*-matrix element, when $0 < (E-E_g) < E_p$. $(E-E_g) \gg E_p$ implies $G_c(E) \rightarrow 1$, recovering the Lorentz oscillator for $\epsilon_2(E)$.

The *novel* normal-incidence transmission, $T_{\Delta d}(\lambda)$, employed in the fitting of the experimental spectrum is:

$$T_{\Delta d}(\lambda) = \frac{A'}{D'}\left(\arctan\left(\frac{C'}{D'}\right) - \arctan\left(\frac{B'}{D'}\right) + \pi\Delta N\right)\frac{x}{\Delta\psi}. \quad (2)$$

The parameters $A', B', C', D', \Delta N, \Delta\psi$, and x are reported by the authors in [5].

4. Results and discussion

Fig. 1*b* shows the top-view-SEM-image of sample #1. It has been suggested that the 'orange peel' effect on the surface occurs because this coating shrinkage reduces the surface energy. Internal stresses cause it during deposition.

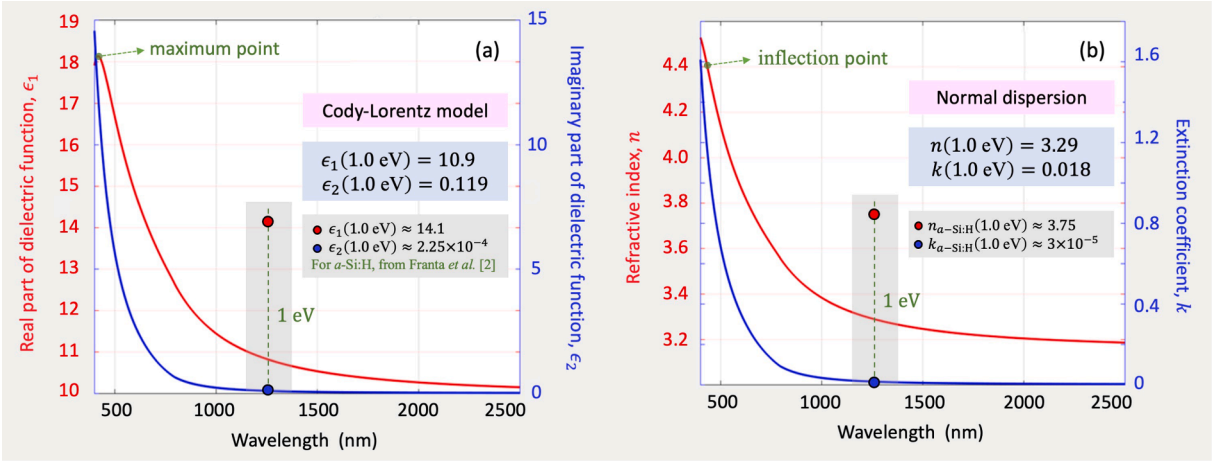

Fig. 3. (*a*) Complex dielectric function and (*b*) refractive index *versus wavelength*.

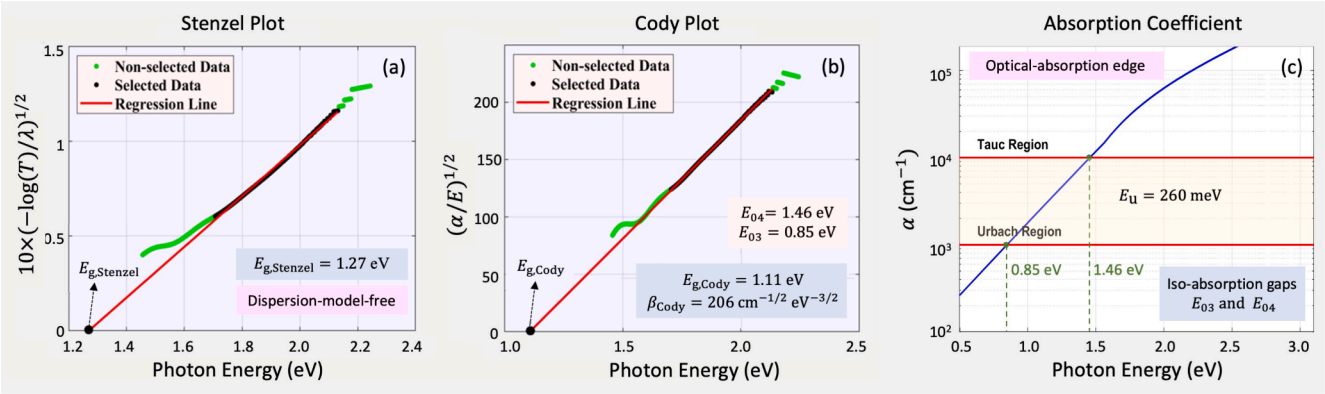

Fig. 4. (*a*) Stenzel's and (*b*) Cody's extrapolations. (*c*) Optical-absorption edge and iso-absorption gaps: Tauc and Urbach regions.

The Raman spectrum is shown in Fig. 1*c* and contains several vibrational phonon modes: the peaks centered at 138, 301, 367, and 460 cm^{-1} are assigned to the transverse-acoustical (TA), longitudinal-acoustical (LA), longitudinal-optical (LO), and transverse-optical (TO) modes, respectively. The TO-peak location is related to the tetrahedral network (sp^3-hybridization).

Fig. 2 shows the *T*-spectra for samples #1 and #2. The best-fit CL parameters belonging to sample #1 were obtained with our Matlab program 'AdjusTransIS': $E_g = 1.07$ eV, $E_u = 260$ meV, $A = 45.4$ eV, $E_0 = 3.83$ eV, $C = 1.60$ eV, $E_t = 1.56$ eV, $E_p = 0.88$ eV, $\overline{d} = 769$ nm, and $\Delta d = 25$ nm. The parameters corresponding to the *uniform-and-thicker* sample #2, $\Delta d = 0$, and $\overline{d} = 1122$ nm are indicated in the GUI in Fig. 2*b*. d_{SEM} for sample #1 is 777 nm, measured by the cross-sectional-SEM-image (Fig. 2*b*).

Following Ferlauto et al. [3], the *offset* was fixed to unity. The agreement between the generated and experimental spectra, with excellent values of the figure-of-merit, FoM, is displayed in both Figs. 2*a* and 2*b*. We found an MSE that is about half of that obtained by the WVASE32 software. We implemented the Nelder-Mead (NM) *heuristic* algorithm instead of the Levenberg–Marquardt *local* optimizer used by the WVASE32. NM can converge to the global minima and avoid undesired local minima in the FoM.

We display ϵ_1 and ϵ_2 for the specimen #1 in Fig. 3*a*. The ϵ_1-peak has a height of 18.1 and is located at 418 nm. The ϵ_2-peak appears at a smaller wavelength, in the region with the 'bumps-and-wiggles' pattern. Fig. 3 illustrates its complex refractive index. For the measured range, *n* is in the normal-dispersion regime. The inflection point is located at 452 nm and anticipates the maximum point and the 'anomalous' dispersion.

Following Stenzel [6], we can find a *quick*-and-*accurate* bandgap estimation. The spectral dependence of α leads to: $\sqrt{\ln(1/T)/\lambda} \propto E - E_{g,Stenzel}$, where $E_{g,Stenzel}$ stands for the 'Stenzel gap', which is equal to 1.27 eV, for sample #1.

α was calculated using only the high-absorption region, where the Fabry–Perot fringes disappear, and its corresponding formula for α [7]. The expression given by Cody [8] $\sqrt{\alpha/E} = \beta_{Cody}(E - E_{g,Cody})$, allows us to find the Cody gap and slope, $E_{g,Cody}$ and β_{Cody}, respectively. Fig. 4*b* shows the Cody plot for sample #1, and the *true* gap, $E_{g,Cody} = 1.11$ eV, as expected, is slightly larger than that of the *nominal* gap, 1.07 eV. This latter gap represents a *mathematical* gap rather than a *physical* one. The *iso-absorption* gaps, $E_{04} = 1.46$ eV and $E_{03} = 0.85$ eV, are also determined and presented in Figs. 4*b* and 4*c*, respectively.

Although not in the scope of the letter, we show that the spectro-ellipsometric results from [9] are consistent with the present finding: The Cody gaps of these *a*-Si layers increase with the Ar-working pressure [10]. It has also been found that the maximum value of *n* decreases with increasing Ar-gas pressure, within the chosen RF-magnetron-sputtering-deposition conditions.

5. Conclusions

a-Si thin films were grown by RFMS onto glass substrates, at a power of 525 W, and Ar-gas-working pressure ranging from 0.7 to 4.5 Pa. Average rates $\gtrsim$1.0 nm/s were achieved. These results do meet the requirements to manufacture low-cost absorbers for photovoltaic cells. We have calculated ϵ_1 and ϵ_2 using the CL model, together with our normal-

incidence transmission formula. Our study highlights the sensitivity of the approach to film non-uniformity, and it can be applied to other non-crystalline and poly-crystalline semiconductors. Δd for sample #1 has been found to be 25 nm, with $d_{\mathrm{SEM}} = 777$ nm. We have corroborated the inverse-synthesis characterizations by comparing all of them with the envelope-method characterizations, see Fig. 2*c*; we calculate $\overline{d} = 782$ nm and $\Delta d = 25$ nm using it. $E_{\mathrm{g,Cody}}$ was found to be 1.1eV (1130 nm), guaranteeing the absorption of the 940-nm-laser radiation.

CRediT authorship contribution statement

E. Marquez: Conceptualization, Methodology, Writing - original draft, Supervision, Funding acquisition. **M. Ballester:** Conceptualization, Methodology, Software, Writing - review & editing. **M. Garcia:** Conceptualization, Methodology, Software, Writing - review & editing. **M. Cintado:** Software. **A.P. Marquez:** Software, Writing - original draft. **J.J. Ruiz:** Conceptualization, Methodology. **S.M. Fernández:** Visualization. **E. Blanco:** Visualization. **F. Willomitzer:** Supervision. **A.K. Katsaggelos:** Writing - review & editing, Supervision.

Declaration of Competing Interest

The authors declare that they have no known competing financial interests or personal relationships that could have appeared to influence the work reported in this paper.

Data availability

Data will be made available on request.

References

[1] M. Ballester, A.P. Márquez, C. García-Vázquez, J.M. Díaz, E. Blanco, D. Minkov, S. Fernández-Ruano, F. Willomitzer, O. Cossairt, E. Márquez, Journal of Non-Crystalline Solids 594 (2022), https://doi.org/10.1016/j.jnoncrysol.2022.121803, 121803.
[2] D. Franta, D. Nečas, L. Zajíčková, I. Ohlídal, J. Stuchlík, Thin Solid Films 541 (2013) 12, https://doi.org/10.1016/j.tsf.2013.04.129.
[3] A. Ferlauto, G.M. Ferreira, J. Pearce, C.R. Wronski, R.W. Collins, X. Deng, G. Ganguly, Journal of Applied Physics 92 (5) (2002) 2424, https://doi.org/10.1063/1.1497462.
[4] G.E. Jellison Jr., F.A. Modine, Applied Physics Letters 69 (3) (1996) 371, https://doi.org/10.1063/1.118064.
[5] J.J. Ruíz-Pérez and E. Márquez. 2020, doi.org/10.3390/coatings10111063. Coatings, 10 (11): 1063.
[6] O. Stenzel, Optical coatings: material aspects in theory and practice, Springer, 2014.
[7] R. Swanepoel, Journal of Physics E: Scientific Instruments 16 (12) (1983) 1214, https://doi.org/10.1088/0022-3735/16/12/023.
[8] G.D. Cody. 1992, doi.org/10.1016/s0022-3093(05)80513–7. Journal of Non-Crystalline Solids, 141: 3.
[9] E. Márquez, E. Blanco, C. García-Vázquez, J.M. Díaz, E. Saugar, Journal of Non-Crystalline Solids 547 (2020) 120305, https://doi.org/10.1016/j.jnoncrysol.2020.120305.
[10] E. Márquez, E. Saugar, J.M. Díaz, C. García-Vázquez, S.M. Fernández-Ruano, E. Blanco, J.J. Ruiz-Pérez, D.A. Minkov, Journal of Non-Crystalline Solids 517 (2019) 32–43, https://doi.org/10.1016/j.jnoncrysol.2019.04.034.